



Compatibility of different measurement techniques of global solar radiation and application for long-term observations at Izaña Observatory

Rosa Delia García^{1,2,3}, Emilio Cuevas¹, Omaira Elena García¹, Ramón Ramos¹, Pedro Miguel Romero-Campos¹, Fernando de Ory¹, Victoria Eugenia Cachorro³, and Angel de Frutos³

¹Izaña Atmospheric Research Centre (IARC), State Meteorological Agency (AEMET), Santa Cruz de Tenerife, 38001, Spain

²Air Liquide España, Delegación Canarias, Candelaria, 38509, Spain

³Atmospheric Optics Group, Valladolid University, Valladolid, Spain

Correspondence to: Emilio Cuevas (ecuevas@aemet.es)

Received: 8 September 2016 – Discussion started: 4 November 2016

Revised: 18 January 2017 – Accepted: 9 February 2017 – Published: 7 March 2017

Abstract. A 1-year inter-comparison of classical and modern radiation and sunshine duration (SD) instruments has been performed at Izaña Atmospheric Observatory (IZO) located in Tenerife (Canary Islands, Spain) starting on 17 July 2014. We compare daily global solar radiation (GSR_H) records measured with a Kipp & Zonen CM-21 pyranometer, taken in the framework of the Baseline Surface Radiation Network, with those measured with a multifilter rotating shadowband radiometer (MFRSR), a bimetallic pyranometer (PYR) and GSR_H estimated from sunshine duration performed by a Campbell–Stokes sunshine recorder (CS) and a Kipp & Zonen sunshine duration sensor (CSD). Given that the BSRN GSR_H records passed strict quality controls (based on principles of physical limits and comparison with the LibRadtran model), they have been used as reference in the inter-comparison study. We obtain an overall root mean square error (RMSE) of $\sim 0.9 \text{ MJm}^{-2}$ (4 %) for PYR and MFRSR GSR_H , 1.9 (7 %) and 1.2 MJm^{-2} (5 %) for CS and CSD GSR_H , respectively. Factors such as temperature, relative humidity (RH) and the solar zenith angle (SZA) have been shown to moderately affect the GSR_H observations. As an application of the methodology developed in this work, we have re-evaluated the GSR_H data time series obtained at IZO with two PYRs between 1977 and 1991. Their high consistency and temporal stability have been proved by comparing with GSR_H estimates obtained from SD observations. These results demonstrate that (1) the continuous-basis inter-comparison of different GSR_H techniques offers important

diagnostics for identifying inconsistencies between GSR_H data records, and (2) the GSR_H measurements performed with classical and more simple instruments are consistent with more modern techniques and, thus, valid to recover GSR_H data time series and complete worldwide distributed GSR_H data. The inter-comparison and quality assessment of these different techniques have allowed us to obtain a complete and consistent long-term global solar radiation series (1977–2015) at Izaña.

1 Introduction

The Earth's radiation budget is essential for driving the general circulation of the atmosphere and oceans, and modulating the main conditions of the Earth's climate system. Several studies have examined the evidence of links between recent changes in climate and in the amount of daily global solar radiation (GSR_H) reaching the Earth's surface, observing a decrease in the GSR_H at the surface between the 1960s and the 1990s, an effect known as dimming (see, e.g., Ohmura and Lang, 1989; Gilgen et al., 1998; Stanhill and Cohen, 2001; Wild, 2009; Wild et al., 2005), with a general decline between 4 and 6 % decade⁻¹ over 30 years considering worldwide distributed stations. In contrast, an increase of the GSR_H between 1 and 10.7 % decade⁻¹ since the 1980s has been documented (e.g. Wild, 2012; Wild et al., 2005, 2007, 2008; Gilgen et al., 2009), known as brightening. However,

for a better understanding of the global effects in the climate system, long-term GSR_H data time series in representative regions are fundamental.

The first solar radiation instruments were designed in the first decade of the last century (Moll, 1913; Chaldecott, 1954; De Bruin et al., 1995; Stanhill, 1998), however, continuous GSR_H observations began in the 1920s at selected locations. The longest known GSR_H data time series have been measured in Stockholm (Sweden) since 1923 (Stanhill and Cohen, 2001), Wageningen (Netherlands) since 1928 (De Bruin et al., 1995) and Potsdam (Germany) since 1937 (Wild, 2015). However, regular and coordinated GSR_H measurements were not well established until the framework of the International Geophysical Year in 1957 and 1958 (IGY, 1957/1958; Nicolet, 1982). The efforts made to increase the knowledge and measurement of the GSR_H led to the necessity to centrally collect the GSR_H measurements. In 1964, the World Meteorological Organization (WMO) established the World Radiation Data Centre (WRDC), which has been operating for over 50 years supported by the Main Geophysical Observatory of the Russian Federal Service for Hydrometeorology and Environmental Monitoring, and centrally collects archives and published radiometric data from several national meteorological and hydrometeorological services and other organisations (WMO, 1965). Furthermore, the increase in the comprehension of the GSR_H influence in the climate system required a homogenisation in the accuracy of the measurements. Thus, several GSR_H measurement networks were established around the world in the early 1990s. In 1992 the Baseline Surface Radiation Network (BSRN; <http://www.bsrn.awi.de>) was created (Heimo et al., 1993; Ohmura et al., 1998). The BSRN is characterised for meeting strict quality control and quality assurance protocols, and consists nowadays of approximately 60 stations in diverse climatic regions across the globe, whose radiation measurements are widely used in climate models and satellite calibration algorithms (Heimo et al., 1993; Ohmura et al., 1998). Other examples are the Atmospheric Radiation Program (ARM; Ackerman and Stokes, 2003), set up in 1992 or the Surface Radiation Budget Network (SURFRAD; Augustine et al., 2000) created in 1993.

Unfortunately, before the establishment of the cited networks, long-term GSR_H data time series were very scarce and not representative for a wide variety of atmospheric conditions. In addition, throughout history, instruments of different types have been used for measuring GSR_H or to obtain indirect estimations of GSR_H , as sunshine duration (SD), with different accuracies, and even different radiometric scales – all this has caused inconsistencies and inhomogeneities in radiation data series, mainly before the 1950s (Fröhlich, 1991). On the other hand, new instruments with better accuracies have regularly replaced older ones, resulting in new uncertainties since in many instrument replacements there were no simultaneous measurements to assess

the compatibility between old and new instruments and the corresponding changes caused in data series.

In order to complete and extend the GSR_H data time series, ancillary measurements are often used to estimate GSR_H . However, it is necessary to know the accuracy of those estimations by comparison with simultaneous GSR_H measurements performed with modern instruments. The SD has been widely used by applying the well-known Ångström–Prescott equation (Ångström, 1924, 1956; Prescott, 1940) to estimate GSR_H . Several authors, such as Almorox et al. (2005), Yorukoglu and Celik (2006) and García et al. (2014b), have used this method in different regions, obtaining similar results. The Robitzsch bimetallic pyranometer (also known as pyranograph or actinograph, hereafter PYR), designed in the early 1920s (Robitzsch, 1926) and widely used until the late 1960s, measures GSR_H from an equation involving the recorded area and the ambient temperature (Robitzsch, 1932). Stravisi (1986) performed a posteriori calibration of a PYR over a 3-year period obtaining hourly, daily and monthly correction factors. Later, Esteves and de Rosa (1989) proposed a correction method to improve the accuracy of daily averaged GSR_H readings, reducing the error from 20 to $\sim 4\%$. Maxwell et al. (1999) performed a comparison between GSR_H estimations from a PYR and GSR_H measurements with an Eppley PSP radiometer. They applied an automatised process to scan the PYR charts finding differences in daily GSR_H values ranging between 2 and 10% over the course of a year.

However, all these partial inter-comparisons were performed in several sites with different environmental conditions, and different instruments and time periods. In contrast, what we propose in this study is to know the performance of different instruments running in parallel in a test-bed site where the environmental conditions show a wide range of variation throughout the year. This allows us to obtain comprehensive and consistent assessments on the GSR_H differences obtained with these instruments.

In this context, this work compares simultaneous ground-based GSR_H measurements performed by different instruments with GSR_H derived from SD and PYR area measurements in order to (1) document the traceability of main solar radiation techniques historically used, and thereby (2) assess their suitability for completing and recovering GSR_H data time series, valid for climate studies. The Izaña Atmospheric Observatory (IZO) is an optimal station to carry out this quality assessment study, since solar radiation observations have been continuously performed since the early 1920s. At IZO, the SD observations started in 1917 with a Campbell–Stokes sunshine recorder (henceforth, CS recorder), which was recently replaced by a Kipp & Zonen sunshine duration sensor (henceforth, CSD recorder). The GSR_H measurements started in 1977 with a PYR and it was replaced in 1992 by different instruments (Kipp & Zonen: CM-5, CM-11 and CM-21). Since 2005, IZO has been a station member of BRN managed by the Spanish National Radiometric Cen-

tre (NRC-AEMET) and since 2009 IZO has been part of the BSRN (BSRN station #61, IZA; García et al., 2012, 2014c). This work is divided into six sections. Section 2 describes the main characteristics of the IZO test site. Section 3 shows the technical description of ground-based instruments and the methodology used to derive the GSR_H estimations from the different observations. Section 4 presents the results obtained in a 1-year intensive campaign ad hoc designed to compare different GSR_H measurement techniques, and in Sect. 5 the GSR_H data time series performed with two pyranometers between 1977 and 1991 at IZO is evaluated. A summary and the main conclusions of this work are given in Sect. 6.

2 Site description

IZO (<http://izana.aemet.es>) is located on the island of Tenerife (Canary Islands, Spain; at 28.3° N, 16.5° W, 2373 m a.s.l.), and is managed by the Izaña Atmospheric Research Centre (IARC), which forms part of the Meteorological State Agency of Spain (AEMET).

IZO is a high-mountain observatory above a strong subtropical temperature inversion layer, which acts as a natural barrier for local pollution, and it provides atmospheric measurements representative of free troposphere conditions of the North Atlantic region due to the quasi-permanent subsidence regime typical of the subtropical region (Cuevas et al., 2013; Gómez-Pelaez et al., 2013). It is optimal for solar radiation measurements given that it has about 3436 h of sunshine per year and a mean annual number of cloud-free days of 221 (61 %) between 1916 and 2015, as well as for calibration and validation activities due to a high atmospheric stability, stable ozone total column amounts, very low column water content and low aerosol concentrations. Due to these privileged measurement conditions IZO has developed a comprehensive atmospheric monitoring programme. In 1984 IZO became a member of the World Meteorological Organization (WMO) Background Atmospheric Pollution Monitoring Network (BAPMoN) and in 1989 it became a Global Atmosphere Watch (GAW) station. Also, it has actively contributed to international radiation networks and databases such as the Network for the Detection of Atmospheric Composite Change (NDACC, <http://www.ndsc.ncep.noaa.gov>) and the Precision Filter Radiometer Network (GAW/PFR, <http://www.pmodwrc.ch/worcc>) since 2001, the Aerosol Robotic Network (AERONET, <http://aeronet.gsfc.nasa.gov>) since 2004, and the BSRN since 2009, among others. Moreover, in July 2014, IZO was appointed by WMO as a CIMO (Commission for Instruments and Methods of Observation) test bed for aerosols and water vapour remote sensing instruments (WMO, 2014).

3 Solar radiation instruments and methodology

In order to compare different GSR_H measurement techniques, all the solar radiation instruments that have historically measured solar radiation at IZO were re-installed at the observatory performing simultaneous observations between 17 July 2014 and 12 July 2015. The installed instruments were a PYR, a CS recorder, a Kipp & Zonen CSD recorder, a multifilter rotating shadowband radiometer (MFRSR) and a CM-21 pyranometer Kipp & Zonen (hereafter BSRN; see Table 1). A CM-21 Kipp & Zonen pyranometer from the BSRN programme was used as reference. In the following sections the different instruments are described as well as the methodology used to derive the GSR_H .

3.1 BSRN station

The GSR_H measurements taken as reference in this study are those from the Izaña BSRN. Since 2009, IZO has been part of the BSRN (#61, IZA; García et al., 2012; <http://www.bsrn.aemet.es/>). The GSR_H at Izaña BSRN is measured with a Kipp & Zonen CM-21 pyranometer (Table 1). Pyranometers integrate radiation hemispherically over a horizontal surface covering a spectral range from 310 to 2800 nm (95 %). The measurements are sampled at 1 Hz, and 1 min mean values are recorded. This instrument has been calibrated recently at the World Radiation Center (WRC) at Davos, Switzerland, and it is regularly compared at IZO with a PMO6 absolute open cavity radiometer (reference instrument) designed at the Physikalisch-Meteorologisches Observatorium Davos (PMOD) following the ISO 9059:1990 (E) and ISO 9846:1993 obtaining less than 0.1 % difference between the given calibration coefficient obtained in WRC and IZO.

The expected uncertainty is $\pm 2\%$ for instantaneous, hourly and daily totals (Ohmura et al., 1998; McArthur, 2005). Similar values were found by García et al. (2014c), they present a comparative study of GSR_H measurements and simulations at BSRN Izaña station. The analysis was based on cloud-free days between March 2009 and August 2012 (386 days), including both aerosol-free and Saharan almost-pure mineral dust conditions. They observed agreement within 99 % and the bias (simulations–measurements) was $-0.30 \pm 0.24 \text{ MJm}^{-2}$ ($-1.1 \pm 0.9\%$) and RMSE of 0.38 MJm^{-2} (1.3 %). However, Stoffel (2005) estimated larger uncertainties for field GSR_H measurements, 10 Wm^{-2} ($\pm 6\%$). These uncertainties are associated with radiometer calibration and measurement system installation, operation and maintenance. The BSRN establishes strict quality controls for shortwave surface radiation and other measurements (Long and Dutton, 2002; Long and Shi, 2006). Applying the BSRN quality controls aforementioned to the Izaña GSR_H measurements for solar zenith angles (SZA) $< 90^\circ$, García et al. (2014c) shows that the measurements largely satisfy the quality control recommended by the BSRN obtaining less than 0.1 % of the measurements out of the physically possi-

ble and extremely rare limits (see Table 1 of García et al., 2014c). Also, other validation of the GSR_H measurements is routinely made by comparison with the LibRadtran model (<http://www.libradtran.org>; Mayer and Kylling, 2005) reporting a high consistency between simulations and measurements of GSR_H (see Table 5 in García et al., 2014c).

3.2 Bimetallic pyranometer

The PYR was designed by Max Robitzsch in 1926 (Table 1), and it was a popular instrument for measuring daily amount of solar irradiance from about 1932 to 1970 at meteorological stations around the world, since it is easy to install and operate and has low maintenance. The pyranometer is based on the properties of a bimetallic strip mounted under a protective glass dome, which bends in response to temperature changes. The different thermal expansion properties of the materials used to form the bimetallic strip create a simple bimetallic thermometer that responds proportionally to changes in solar irradiance (Vignola et al., 2012). By coating the strip with a black absorbent material and exposing it to the Sun's energy, the strip bends in proportion to the change in temperature, which is proportional to the intensity of the solar radiation. The signal is instantaneously recorded in a strip card, being the area under the radiation curve proportional to the incoming solar radiation. The measurement uncertainties introduced by a variety of undesirable response characteristics result in daily solar irradiance within $\pm 20\%$ for the best-performing instruments (Coulson, 1975; Garg and Garg, 1993). For this reason this instrument was classified by WMO as a third-class pyranometer (WMO, 1965).

In order to convert the area obtained from the pyranometer strip card to radiation units the following equation is used:

$$Q = K S (1 + 0.0033 \bar{t}), \quad (1)$$

where K is the instrument constant, S is the value of the integrated surface (area) in cm^2 and \bar{t} is the averaged temperature in $^{\circ}\text{C}$ from temperature observations at 07:13:18 UTC. Q is expressed in $\text{cal cm}^{-2} \text{min}^{-1}$. The constant K is dependent on each instrument; unfortunately this constant is unknown for the instrument used in this work. Therefore, we have estimated the constant K from Eq. (1) considering that Q is the theoretical GSR_H. In particular, we have calculated a K value for each month considering only cloud-free days. These days were selected using Long and Ackerman's method (Long and Ackerman, 2000). Hereafter, the GSR_H estimations with this method are denoted PYR-1 GSR_H.

Also, we have used a second approach, the Esteves method (Esteves and de Rosa, 1989), to determine the GSR_H performed with the pyranometer (hereafter, PYR-2 GSR_H). This method defines a monthly factor (F_m) that is determined for a given set of cloud-free days of the same month as the sum of ratios between the theoretically calculated daily GSR_H value and the area of the register for the same day, divided by the

number of days in the set:

$$F_m = \frac{\sum_{i=1}^{n_m} \frac{H_{ci}}{S_i}}{n_m}, \quad (2)$$

where H_{ci} is the theoretical GSR_H for the clear day i , S_i is the area inscribed under the registered curve for the day i and n_m is the number of clear days of the month considered. Once the value of the monthly factor is obtained, it is possible to calculate the daily GSR_H for any day of the month as follows:

$$\text{GSR}_H = F_m S, \quad (3)$$

where S is the area inscribed under the register's curve for a given day of the month (idem to Eq. 1). GSR_H is expressed in MJm^{-2} .

For the two methods, two variables are needed to be calculated: the theoretical GSR_H (Q in PYR-1 and H_{ci} in PYR-2) and the area S . Firstly, the theoretical GSR_H was calculated using the LibRadtran model (see Sect. 3.1). To simulate the GSR_H values, we used daily aerosol optical depth (AOD) data from AERONET (Holben et al., 1998) and precipitable water vapour (PWV) observations from Vaisala meteorological radiosondes (Miloshevich et al., 2009), launched at Güimar (WMO station #60018) at 11:15 UTC (Romero Campos et al., 2011). Further details about the LibRadtran simulations can be found in García et al. (2014c).

The area, S , was calculated by using a semiautomatic method ad hoc developed at IZO to digitalise the data recorded on the pyranometer strip cards. Figure 1 shows the flow chart illustrating the methodology used on 10 August 2014, as an example. The processing is performed using the MATLAB Image Processing Toolbox (Russ, 1994). Firstly, each strip card is scanned with a resolution of 300 ppi and saved to 24 bit RGB TIF (Tagged Image Format). The image is trimmed in order to only include the radiation curve in the image, discarding possible spurious notations and the signals on the strip card. In a few cases, minor editing of the trimmed image is needed to clean it of spots and defects. A median filter is applied to the trimmed image and two background areas are selected (Fig. 1.3), normally in the upper corners of the image. For each channel (R, G and B) a statistical analysis is performed on the background areas in order to establish the thresholds needed to define the pixels that belong to the curve. Once the curve pixels are identified we extract the coordinates in pixel units and the curve is smoothed to detect the sunrise and sunset points using the Savitzky–Golay algorithm (Gorry, 1990; Fig. 1.6). With the pixel coordinates of the sunrise and sunset we construct a straight line connecting both points. Finally the area, S , in pixels^2 is obtained by calculating the area bounded between the radiation curve and the base line. Taking into account that the resolution of the image is 300 ppi, dividing the area S in pixels^2 by 13 950, the area in cm^2 is obtained.

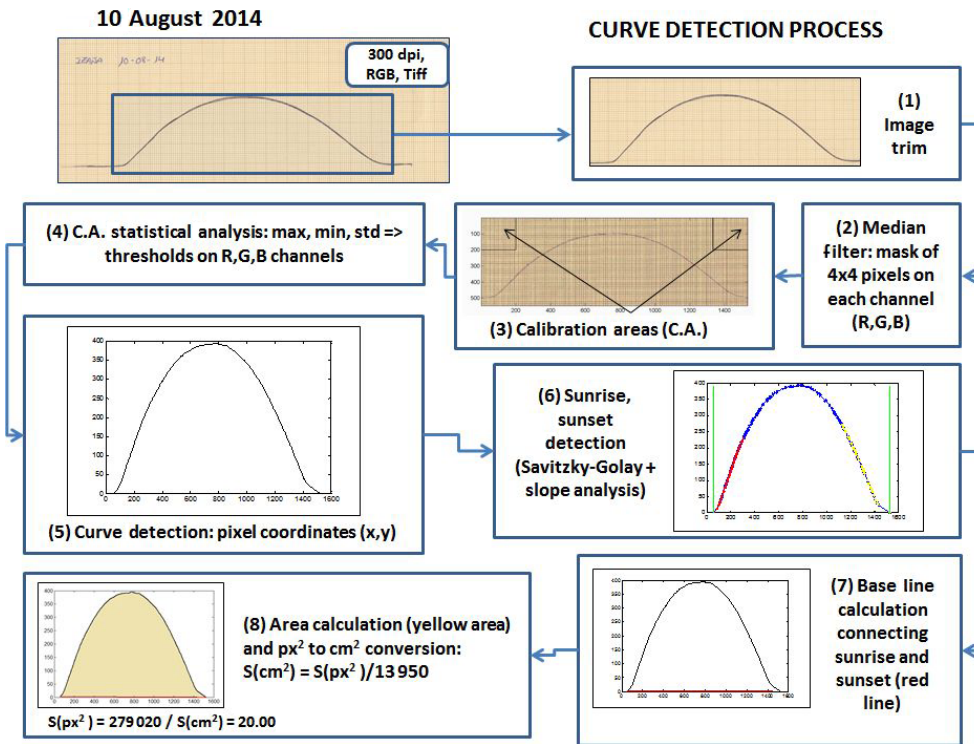


Figure 1. Flow chart of the method used to extract the areas from the strip cards of the bimetallic pyranometer.

Table 1. Characteristics and uncertainties of each solar radiation instrument used: Robitzsch bimetallic pyranometer (PYR), Campbell–Stokes sunshine recorder (CS recorder), Kipp & Zonen sunshine duration sensor (CSD recorder), multifilter rotating shadowband radiometer (MFRSR) and pyranometer CM-21 Kipp & Zonen (BSRN) installed between 17 July 2014 and 12 July 2015 at IZO.

	Bimetallic Pyranometer	CS recorder	CSD recorder	MFRSR radiometer	CM-21 Kipp & Zonen Pyranometer
Instrument pictures at IZO					
Magnitude	Area (cm ²)	SD (hours)	SD (hours)	GSR_E (Wm ⁻²) (300–1100 nm)	GSR_E (Wm ⁻²) (280–2600 nm)
Uncertainty	±5 to 10 %	±9 %	±5 %	< 5 %	≈ 2 %
Reference	Garg and Garg (1993)	García et al. (2014b)	García et al. (2014a)	Hodges and Michalsky (2011)	Ohmura et al. (1998)

We have also computed the instantaneous GSR_H values from the pyranometer radiation curve. The conversion of the horizontal axis from pixels to time is straightforward by taking into account the relation between the distance in pixels and time from sunrise to sunset throughout the day. The vertical conversion requires more effort due to the clear dependence of the calibration factors on month and hour, as pointed to in previous works (Albrecht, 1954; Stravisi, 1986). Thus, assessment of calibration factor dependence on the mentioned variables is required. In order to convert from cm

to Wm⁻² the next relation is proposed:

$$GSR_H \text{ PYR (Wm}^{-2}\text{)} = C \text{ (month, minute)} Y \text{ (mm)}, \quad (4)$$

where Y is obtained in the image processing method already discussed and C are coefficients computed with the LibRad-tran model which has demonstrated to be a very useful measurement quality control tool (García et al., 2014c). This study is performed for a sample of cloud-free days in May and June (2015), a month in which there is a maximum SZA range.

3.3 Sunshine recorders: CS and CSD

The CS recorder was invented by J. F. Campbell in 1853 and modified to its usual shape by G. G. Stokes in 1879 (Table 1). The CS focuses the direct solar beam through a glass sphere, mounted concentrically in a section of a spherical bowl, on a burn card located under the sphere. The card is provided with a time indication, which makes it possible to determine the SD from the length of burn when the card is removed from the instrument at the end of the day (Painter, 1981; WMO, 1996; Sanchez-Lorenzo et al., 2013; García et al., 2014a, b). The errors of this recorder are mainly due to the dependence of burning initiation on card's temperature and humidity as well as to the overburning effect, especially in the case of broken clouds (Kerr and Tabony, 2004).

The CSD recorder (Table 1) was designed with the objective of automating the process of measuring SD for meteorological services and has replaced the traditional CS recorders. This instrument is formed by three detectors: the sensor at the front measures global radiation, while the other two detectors, at the middle and at the rear, are partially shaded covering 1/3 of the sky, measuring diffuse radiation (Kipp and Zonen, 2003). Furthermore, the three detectors have exactly the same spectral and angular characteristics, making the process of calibration easy. The direct solar radiation can be computed from the values of global and diffuse solar radiation, and the sunshine duration is determined according to the latest WMO definition (WMO, 1996).

In this work, the method used to determine the GSR_H estimated from SD records was developed by Ångström (Ångström, 1924, 1956) and later modified by Prescott and Rietveld (Prescott, 1940) and applies the following equation:

$$\frac{H}{H_o} = a \frac{n}{N_d} + b, \quad (5)$$

where H and H_o are the daily GSR_H and the daily extraterrestrial GSR_H ($\text{MJm}^{-2} \text{day}^{-1}$), respectively, on a horizontal surface, n and N_d are the number of hours measured by the SD recorder and the maximum daily SD, respectively, and a and b are coefficients to be determined by using linear regression.

This method has successfully been validated at IZO by García et al. (2014a, b), obtaining an expected uncertainty of 9.2 % for CS recorder and 5.5 % for CSD recorder when comparing BSRN GSR_H . Following Eq. (5) and details given in García et al. (2014a, b), the a and b coefficients at IZO are given in Table 2 for each SD recorder. To account for the variability introduced by the presence of clouds, fog, etc., these coefficients were estimated as functions of the fraction of clear sky (FCS), which is defined as the ratio between the maximum daily sunshine duration N_d and SD performed with CS recorder (n):

$$\text{FCS}(\%) = \frac{n}{N_d} \times 100. \quad (6)$$

Table 2. The a and b coefficients obtained between 1992 and 2000 for the CS recorder and between 2001 and 2013 for the CSD recorder, as a function of FCS (fraction of clear sky, %) and % of days used (see García et al., 2014b). SEM is standard error of the mean.

FCS (%)	$a \pm \text{SEM}$	$b \pm \text{SEM}$	% days
CS: 1992/2000			
≤ 20	0.304 ± 0.120	0.347 ± 0.012	9
20–40	0.449 ± 0.144	0.348 ± 0.050	5
40–60	0.516 ± 0.085	0.325 ± 0.048	8
60–80	0.402 ± 0.041	0.399 ± 0.033	23
≥ 80	0.475 ± 0.039	0.339 ± 0.038	55
CSD: 2001/2013			
≤ 20	0.642 ± 0.140	0.281 ± 0.015	3
20–40	0.664 ± 0.111	0.258 ± 0.038	5
40–60	0.577 ± 0.074	0.273 ± 0.042	5
60–80	0.447 ± 0.044	0.362 ± 0.036	11
≥ 80	0.719 ± 0.016	0.109 ± 0.016	76

3.4 MFRSR radiometer

The MFRSR (Table 1) was developed in the early 1990s. This radiometer uses independent interference-filter photodiode detectors and the automated rotating shadowband technique to make spectrally resolved measurements at seven channels with six wavelength passbands of 10 nm FWHM centred near 415, 500, 610, 665, 862 and 940 nm, and an unfiltered channel used to obtain broadband solar irradiance estimates from 300 to 1100 nm. Each measurement sequence is routinely repeated every 15 s and the recorded instantaneous signals are subsequently averaged over a 1 min time interval to increase the signal-to-noise ratio (Harrison et al., 1994).

In this work, the MFRSR was re-calibrated using the LibRadtran model obtaining a new calibration factor calculated as the mean of ratio between the GSR_H measurements and simulations in a time interval of 5 min before and after the solar noon (WMO, 1996), only considering cloud-free days (160 days, 44 %). The obtained calibration factor was 0.438 ± 0.008 .

Although the MFRSR provides the GSR_H directly, the spectral range covered by this instrument (300–1100 nm) is significantly smaller than that of the reference instrument used, the CM-21 pyranometer (280–2600 nm). For this reason, we have calculated a radiation correction using the LibRadtran model as a linear relation between the GSR_H in the MFRSR and the CM-21 spectral ranges. We have modelled the same days selected to calculate the calibration factor in both spectral ranges with the same input values, obtaining a very good agreement (correlation coefficient, R , of 0.995) and the following fit equation:

$$GSR_{280-2600} = (1.239 \pm 0.006)GSR_{300-1100} + (0.4247 \pm 0.014). \quad (7)$$

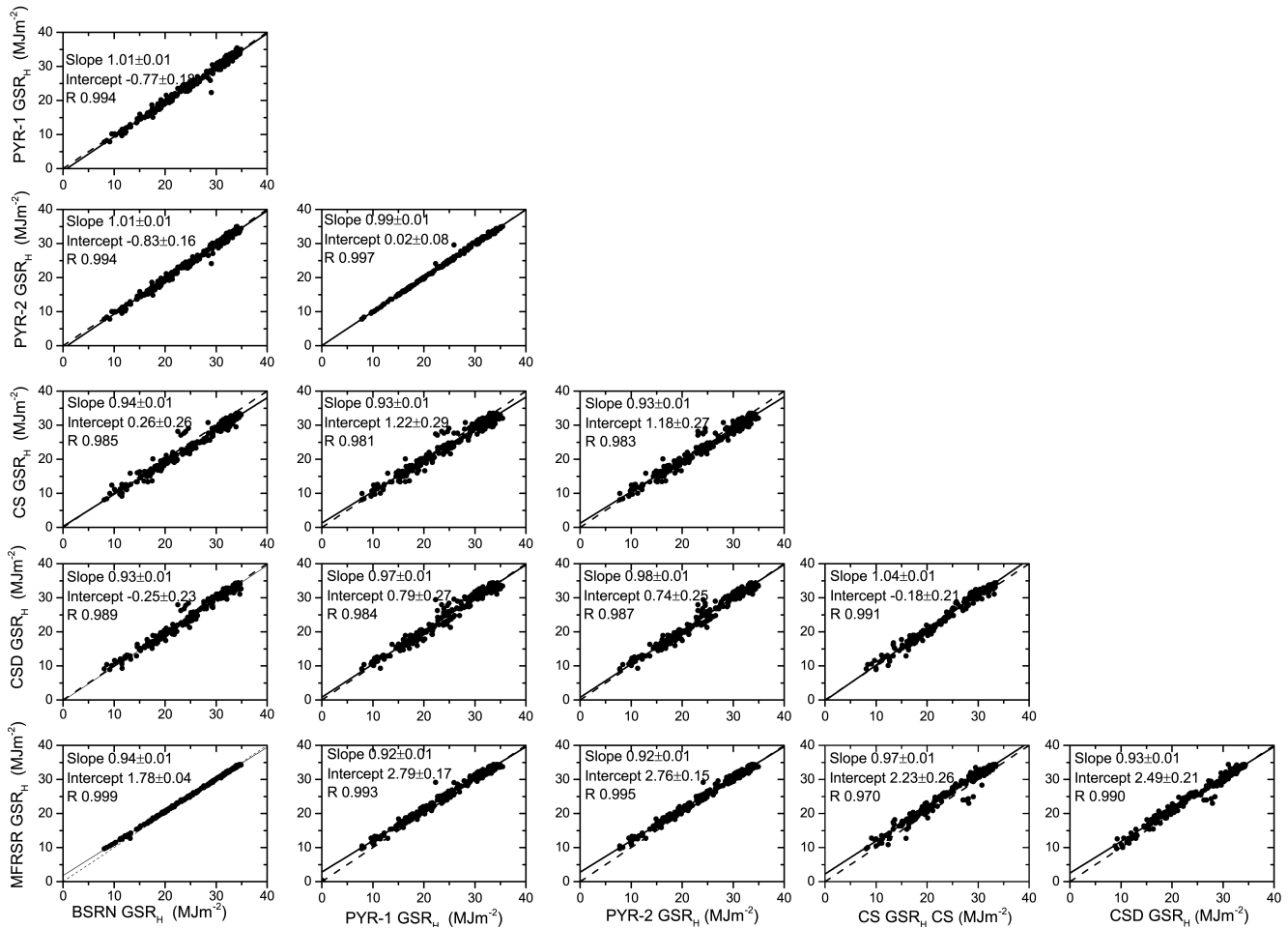


Figure 2. Scatterplot of daily GSR_H (MJm⁻²) performed with CM-21 (BSRN), pyranometer (PYR) determined from Method 1 (PYR-1) and Method 2 (PYR-2), CS recorder, CSD recorder and MFRSR radiometer between 17 July 2014 and July 2015 at IZO ($N = 272$ days). The black solid lines are the least-squares fits and the dotted lines are the diagonals ($x = y$). The least-squares fit parameters are shown in the legend (slope, intercept and correlation coefficient R). N : 272 days.

4 Results

In this section we present the comparison of the daily GSR_H values obtained with the different instruments and techniques using BSRN as reference and we also perform an analysis of the GSR_H bias as a function of the season, solar irradiance, temperature, relative humidity (RH), FCS and AOD. In addition, we present the comparison of the instantaneous GSR_H values measured with PYR and MFRSR with respect to BSRN.

4.1 Comparison of daily GSR_H data

Applying the different methodologies discussed in the previous section, we have computed the daily GSR_H values from the different instruments and techniques between 17 July 2014 and 12 July 2015 at IZO. The daily GSR was calcu-

lated according to the following equation:

$$\text{GSR}_H = \int_{\text{sr}}^{\text{ss}} \text{GSR}_E(t) dt, \quad (8)$$

where $\text{GSR}_E(t)$ is the instantaneous value of the solar irradiance (Wm^{-2}) at time (t), computed from sunrise (sr) to sunset (ss).

In general, as expected, the best agreements with BSRN GSR_H (with $R = 0.999$) are found for those instruments that directly measure solar radiation (not estimations) and have been calibrated with the LibRadtran model, since the model has been widely validated against the BSRN measurements at IZO (García et al., 2014b). Although the poorest scores are those provided by GSR_H estimations from CS measurements ($R = 0.978$), it is worth emphasising that the correlation coefficient is always greater than 0.97 and the slope ranges between 0.92 and 1.04 for all cases. The correla-

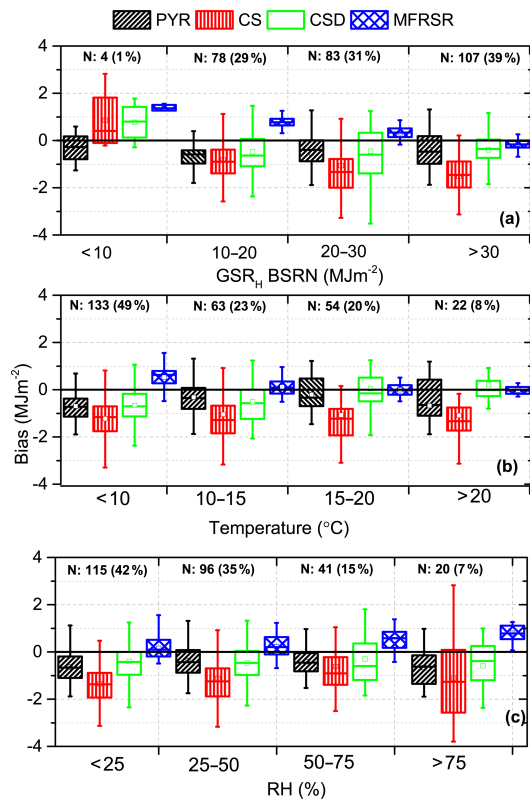


Figure 3. Box plot of bias (PYR: black; CS: red; CSD: green; and MFRSR: blue) versus (a) corresponding BSRN GSR_H measurements (MJm^{-2}), (b) temperature in $^{\circ}C$ and (c) relative humidity (RH) in % between 17 July 2014 and 12 July 2015 at IZO. Lower and upper boundaries for each box are the 25th and 75th percentiles, the solid line is the median value, and hyphens are the maximum and minimum values. N indicates the number the measurements in each season.

tion between PYR-1 GSR_H and PYR-2 GSR_H is very good, with $R = 0.997$. Results of comparison of the instruments are shown in Fig. 2.

In order to quantify the uncertainty of the different techniques with respect to BSRN GSR_H , we have calculated the absolute difference or bias ($XXX\ GSR_H - BSRN\ GSR_H$, in MJm^{-2}) and the relative difference ($(XXX\ GSR_H - BSRN\ GSR_H)/BSRN\ GSR_H$, in %), where XXX means PYR, CS, CSD and MFRSR. As a summary, Table 3 lists the metrics used to quantify these measurements (MB: median bias; SD: standard deviation; and RMSE: root mean square error). In general, GSR_H is underestimated, except for GSR_H MFRSR. The results obtained for PYR-1 and PYR-2 GSR_H are very similar with MB of $-0.5\ MJm^{-2}$ (-2%), while the precision, given by the RMSE, is of $0.9\ MJm^{-2}$ (3.5%) for both cases. The greatest difference is obtained for the CS GSR_H , with MB of $-1.14\ MJm^{-2}$ (-4.5%) and RMSE of $1.70\ MJm^{-2}$ (6.7%). The MFRSR GSR_H is slightly overestimated with a MB of $0.28\ MJm^{-2}$ (1.1%) and RMSE of $0.54\ MJm^{-2}$ (2.1%). Since the results obtained by PYR 1

and PYR-2 are similar, hereafter we will discuss only the results of the PYR-1 – renamed as PYR.

As aforementioned, some of the instruments and methods analysed are sensitive to different factors and atmospheric conditions. We have analysed the GSR_H differences with respect to BSRN GSR_H as a function of the solar irradiance (Fig. 3a), the average temperature and RH (Fig. 3b and c, respectively), the FCS and AOD.

The PYR GSR_H estimations do not show dependence on solar irradiance (Fig. 3a) with a MB almost constant around $-0.5\ MJm^{-2}$. The PYR GSR_H shows a slight dependence on temperature with the lowest MB in the $10\text{--}20\ ^{\circ}C$ range (Fig. 3b) which agrees with the seasonal variation, considering that the highest median temperatures are found in summer and autumn at IZO. This behaviour was also observed by Stravisi (1986) and Esteves and de Rosa (1989) and is attributed to the response of the bimetallic strips to temperature changes (see Sect. 3.2), since the optimum operating temperature is around $15\ ^{\circ}C$. Figure 3c shows that there is not a clear dependence on RH.

The CS GSR_H estimations show a clear dependence on solar irradiance, with higher bias for higher BSRN GSR_H values. However, there is no temperature dependence, with an almost constant bias value around $-1\ MJm^{-2}$ (Fig. 3b), and a slight dependence on RH, with higher bias for the lower RH values (Fig. 3c). This might be explained by the fact that a card requires more solar irradiance to be burnt under wetter conditions, as frequently occurs in early morning (Bider, 1958), while it burns more easily under warm and dry conditions (Kerr and Tabony, 2004; Painter, 1981). Thus, overburning of the card in spring and summer seasons is to be expected.

The CSD GSR_H estimation, unlike CS GSR_H , shows much lower bias, with an opposite annual cycle to that found for CS GSR_H , with higher GSR_H bias in winter and autumn, and lower in spring and summer. Although a slight dependence on solar irradiance is observed, this is much lower than in the case of CS GSR_H (Fig. 3a). There is a slight dependence on temperature, with higher negative bias for lower temperatures (Fig. 3b) and a MB close to zero for temperatures $> 20\ ^{\circ}C$. The manufacturer declares a temperature dependence of $0.1\ \%/^{\circ}C$ (Kipp and Zonen, 2003). There is no dependence on RH (Fig. 3c).

Finally, the MFRSR is the instrument that shows the best performance, with a bias close to zero through the whole year, and the lowest scatter (Fig. 3). We observe, in general, an overestimation in MFRSR GSR_H , unlike the rest of the compared instruments. The MFRSR GSR_H has a clear positive dependence on solar irradiance (Fig. 3a). There is no temperature dependence for temperatures $> 15\ ^{\circ}C$, (Fig. 3c) and a slight dependence for lower temperatures. The MFRSR is thermally controlled at around $40\ ^{\circ}C$. Thus, when the difference between ambient temperature and $40\ ^{\circ}C$ is very large, the heating system is continuously working at 100% effort, creating in former MFRSR instrument versions an electro-

Table 3. Statistics of the comparison between daily GSR_H from PYR (Method 1 and 2), CS recorder, CSD recorder and MFRSR with daily BSRN GSR_H (XXX GSR_H – BSRN GSR_H) at IZO between 17 July 2014 and 12 July 2015 (in MJm⁻²). MB, median bias; SD, standard deviation; MAB, mean absolute bias; and RMSE, root mean square error; statistics percentages in parentheses.

	MB	SD	RMSE	MAB
PYR-1/BSRN GSR _H	-0.50 (-1.9 %)	0.73 (4.3 %)	0.88 (3.5 %)	0.74 (2.9 %)
PYR-2/BSRN GSR _H	-0.54 (-2.2 %)	0.66 (4.5 %)	0.86 (3.4 %)	0.70 (2.8 %)
Cs/BSRN GSR _H	-1.15 (-4.4 %)	1.46 (6.4 %)	1.86 (7.1 %)	1.58 (6.2 %)
CSD/BSRN GSR _H	-0.41 (-1.5 %)	1.17 (5.2 %)	1.23 (4.7 %)	0.91 (3.5 %)
MFRSR/BSRN GSR _H	+0.76 (+3.2 %)	0.53 (2.7 %)	0.93 (3.8 %)	0.82 (3.4 %)

Table 4. Statistics for the bias between instantaneous GSR_E performed with PYR and MFRSR with respect to BSRN GSR_E (XXX GSR_E – BSRN GSR_E) at IZO between May and June 2015 (27 cloud-free days) (in Wm⁻²) for different range of SZA. MB, median bias; SD, standard deviation; and RMSE, root mean square error. Statistics for the relative bias are in parentheses.

	Range of SZA (°)	MB	SD	RMSE
PYR/BSRN GSR _E	< 10°	-31.40 (-2.8 %)	10.77 (0.9 %)	33.19 (3.0 %)
	10–20°	-31.03 (-2.9 %)	17.72 (1.6 %)	35.75 (3.3 %)
	20–30°	-23.27 (-2.3 %)	21.71 (2.1 %)	31.82 (3.1 %)
	30–40°	-15.82 (-1.7 %)	25.32 (2.8 %)	29.85 (3.3 %)
	40–50°	-11.31 (-1.4 %)	33.16 (4.2 %)	35.03 (4.5 %)
	50–60°	-5.64 (-0.9 %)	46.31 (7.5 %)	46.64 (7.4 %)
MFRSR/BSRN GSR _E	< 10°	-0.34 (0.1 %)	6.47 (0.6 %)	6.48 (0.6 %)
	10–20°	-1.36 (-0.1 %)	8.79 (0.8 %)	8.89 (0.8 %)
	20–30°	-1.96 (-0.2 %)	12.17 (1.2 %)	12.33 (1.2 %)
	30–40°	0.34 (0.1 %)	14.33 (1.6 %)	14.33 (1.6 %)
	40–50°	-0.35 (0.1 %)	17.70 (2.3 %)	17.70 (2.3 %)
	50–60°	0.85 (0.1 %)	19.46 (3.1 %)	19.48 (3.1 %)

magnetic frequency interference with the solar irradiance measurements, leading to higher measurement inaccuracies (Harrison et al., 1994; Hodges and Michalsky, 2011). The MFRSR GSR_H measurements show a slight positive dependence on RH (Fig. 3c).

We have also studied the differences with respect to FCS and AOD (not shown here). No dependence on FCS was found, although it should be noted that 85 % of the days (*N*: 232 days) showed FCS > 75 % while only 1 % (*N*: 4 days) showed FCS < 25 %. Concerning the dependence on AOD only background conditions (AOD < 0.10) and dust conditions (AOD ≥ 0.10) have been considered based on García et al. (2014b). No dependence on AOD is found, although we must highlight the fact that 87 % of the days (*N*: 231 days) showed AOD < 0.10 and 13 % of the days (*N*: 33 days) showed AOD ≥ 0.10. The GSR_H measurements most affected by AOD were those obtained with the CSD, showing negative bias for pristine skies and positive bias for dust conditions.

4.2 Diurnal GSR_E comparison

This section presents the diurnal comparison of the instantaneous GSR_E values from PYR and MFRSR (the only instru-

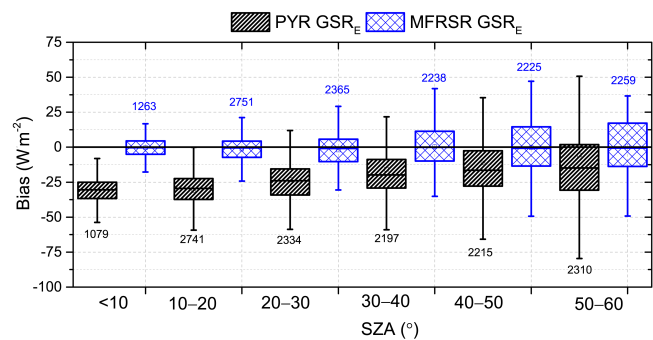


Figure 4. Box plot of the bias (PYR: black; MFRSR: blue) with respect to BSRN GSR_E in Wm⁻² at different ranges of SZA between May and June 2015 (27 cloud-free days) at IZO. Box plots are defined as in Fig. 3.

ments that have this information) with those of the BSRN, used again as reference, applying the methodology discussed in Sect. 3.2. We have considered 27 cloud-free days between May and June 2015, grouping them into intervals of SZA from 10 to 60° (Table 4, Fig. 6). The results show that the GSR_E MB decreases with the SZA for PYR GSR_E, while

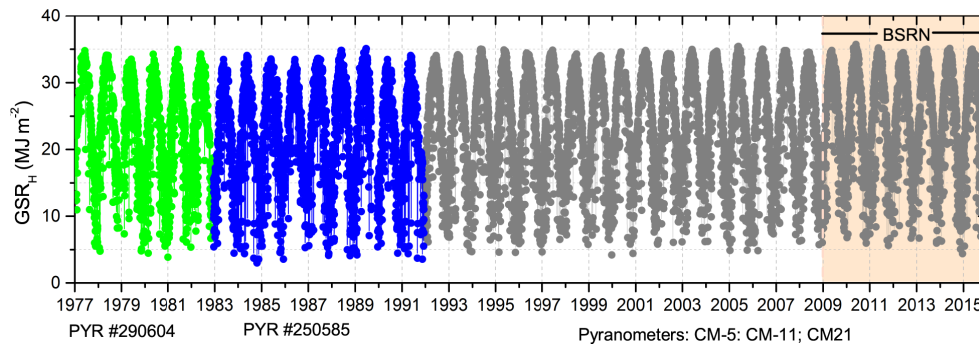


Figure 5. Daily GSR_H data time series between 1977 and 2015 at IZO. The green and blue dots correspond to the measurements performed with PYR #290609 and #250585, respectively, between 1977 and 1991, and the grey dots represent the measurements performed with different pyranometers (CM-5, CM-11 and CM-21) between 1992 and 2015.

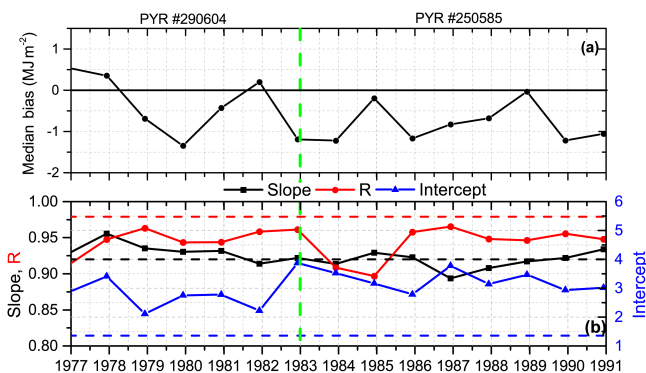


Figure 6. (a) Time series of the median bias between PYR GSR_H and CS-AP GSR_H in MJm^{-2} , and (b) time series of the slope (black line), correlation coefficient (red line; R) and intercept (blue line) for each year. The black, red and blue dashed lines indicate the slope, R and intercept obtained in the period 2014–2015, respectively (see Fig. 3). The green dashed lines represent the instrument change in 1983.

MB is quite stable for MFRSR GSR_E values (Table 4 and Fig. 6). In both cases the SD increases notably with SZA .

5 1977–1991 Time series

As an application of the previous analysis, we have applied the methodology explained in Sect. 4.1 to the measurements performed at IZO between 1977 and 1991 with two bimetallic pyranometers: (1) #290604 (1977–1982), and (2) #250585 (1983–1991). The theoretical GSR_H needed to obtain the instrument constant (K in Eq. 1, $PYR-1 GSR_H$) in these periods was calculated using the LibRadtran model, where the main model inputs were the AOD and PWV. Given that there are no available AOD measurements, we have used AOD derived from artificial neural networks (ANNs) applying the methodology developed by García et al. (2016). The PWV between 1977 and 1979 was taken

from the NCEP/NCAR reanalysis (Kalnay et al., 1996) and since 1980 we have used the PWV obtained from meteorological radiosondes (Miloshevich et al., 2009), and specifically those launched from Santa Cruz de Tenerife station (WMO#60020). Once the instrument constants were evaluated we calculated the GSR_H from the PYR measurements. By combining the re-evaluated GSR_H data time series between 1977 and 1991 from PYR measurements and the GSR_H series measured with different pyranometers from 1992 to 2015, obtained in García et al. (2014b), we finally completed the 38-year GSR_H data time series at IZO, depicted in Fig. 5.

In order to analyse the suitability of the PYR measurements to fill gaps in long-term GSR_H data time series, we have studied the temporal stability of the PYR data time series at IZO between 1977 and 1991 by comparing two independent GSR_H data series. During that period, the only available GSR_H data at IZO are those estimations from CS records, presented in García et al. (2014b). That work presented the re-evaluation of the GSR_H data time series between 1933 and 1991 from SD measurements performed with a CS by using the Ångström–Prescott method, and documented also its high quality and temporal consistency. Hereafter, we refer to that data time series as CS-AP GSR_H to distinguish it from the CS GSR_H obtained in the current study.

In general, there is a good agreement between PYR GSR_H and CS-AP GSR_H (Fig. 6a), being both GSR_H data time series very consistent with each other, with correlation coefficient of 0.86. To check the temporal stability of PYR GSR_H observations, we examine possible drifts and discontinuities in the MB data time series ($PYR GSR_H - CS-AP GSR_H$), considering a drift as the linear trend of the annual MB, while the change-points (change in the median of the bias time series) are analysed by using a robust rank order change-point test (Lanzante, 1996). We found that there are no significant drifts in the MB time series and no change-points are found at 99 % level of confidence. To complete this analysis, we ex-

amined the temporal evolution of the annual transfer function between PYR GSR_H and CS-AP GSR_H , shown in Fig. 6b. This is calculated as the annual slope and intercept considering all the PYR GSR_H and CS-AP GSR_H observations for each year. As for MB, neither temporal drifts nor significant discontinuities were detected at 99 % confidence level for any of the least-squares-fit parameters.

The slope values are higher than 0.88 for all the years, with the median value of 0.92, coincident with that obtained between PYR GSR_H and CS GSR_H for the 2014–2015 period (Fig. 2). The intercept in the period 1977–1991 is higher than in the 2014–2015 period, while the R values are of about 0.95 in the whole period, and 0.98 in the 2014–2015 period. This improvement is likely due to the cleaning and fitting of the instrument before being restarted for the 2014–2015 inter-comparison.

6 Summary and conclusions

A 1-year-long comparison (17 July 2014 to 12 July 2015) between GSR_H measurements performed with old and modern radiation and sunshine duration instruments has been performed at IZO. The daily GSR_H values measured with a bimetallic pyranometer (PYR) and multifilter rotating shadowband radiometer (MFRSR), and GSR_H estimated from SD performed by a Campbell–Stokes sunshine recorder (CS) and a sunshine duration sensor (CSD) have been compared with respect to GSR_H from a BSRN CM21 pyranometer. We have also compared instantaneous values of GSR_H performed with PYR and MFRSR for different SZA with respect to GSR_H BSRN.

Assuming BSRN GSR_H as reference, the measured or estimated GSR_H values show median biases of 2 and 1 % for PYR and MFRSR GSR_H , respectively, and of 5 and 2 % for CS and CSD GSR_H , respectively. These results, as expected, show that the instruments that directly measure GSR_H , such as the PYR and MFRSR, show lower MB and lower scatter than the ones that estimate the GSR_H , such as the CS and CSD recorders. Moreover, MB values for each instrument are within their corresponding uncertainty, agreeing with results obtained by other authors (Coulson, 1975; García et al., 2014b; McArthur, 2005). The comparison of the daily GSR_H values from PYR and MFRSR showed a good agreement with BSRN GSR_H , obtaining a RMSE of ~ 0.9 (3 %) and ~ 0.5 MJm^{-2} (2 %) for PYR and MFRSR GSR_H , respectively, and ~ 1.7 (7 %) and ~ 1.1 MJm^{-2} (4 %) for CS and CSD GSR_H , respectively. It is worth highlighting the fact that the biases for PYR found in this study are lower than those reported by others authors. For example, Coulson (1975) and Garg and Garg (1993) obtained uncertainties between 10 and 20 % reduced up to 4–5 % by Esteves and de Rosa (1989) and Soulayman and Daudé (1995). These results, obtained with simultaneous observations under the same environmental conditions, provide information

about expected GSR_H uncertainties from historical instruments useful for assessing long-term GSR_H data series constructed from both classical and modern instruments.

The GSR_E from PYR and MFRSR were compared with GSR_E BSRN on a daily basis at different solar zenith angles. The RMSE increases from 3 to 7 %, and from 0 to 3 % for PYR and MFRSR GSR_E , respectively, when the SZA increases.

The methodology developed in this work has allowed us to obtain a unique re-evaluated and quality-assured GSR_H data time series from 1977 to 1991 at IZO using GSR_H data from two bimetallic pyranometers. The consistency in the obtained daily GSR_H PYR is good with respect to the daily GSR_H estimates from SD measurements with a correlation coefficient of 0.86.

These results demonstrate that (1) the continuous inter-comparison of different techniques used to measure GSR_H constitutes an important diagnostics tool for identifying inconsistencies between GSR_H data records, and (2) GSR_H measurements performed with classical and simple instruments are fundamental for filling gaps in long-term GSR_H data series after accurate data screening, calibration and correction by using ad hoc reanalysis techniques based on transference radiative models.

7 Data availability

The daily GSR_H data time series for the period 1977–2015 at IZO are available at <http://izana.aemet.es/dataseries/GSR>.

Competing interests. The authors declare that they have no conflict of interest.

Acknowledgements. This study forms part of the activities carried out within WMO CIMO Testbed for Aerosols and Water Vapour Remote Sensing Instruments at Izaña Observatory. The authors are grateful to the IZO team and especially all observers who have worked in the past 70 years taking bimetallic pyranometer measurements at IZO as well as all members of security staff who have helped make this work possible.

Edited by: O. Dubovik

Reviewed by: three anonymous referees

References

- Ackerman, T. P. and Stokes, G. M.: The atmospheric radiation measurement program, *Phys. Today*, 56, 38–44, doi:10.1063/1.1554135, 2003.
- Albrecht, F. H. W.: Establishment of a radiation network connected to ordinary weather stations and evaluation of their observations, *Geofisica pura e applicata*, 29, 115–154, doi:10.1007/BF01988608, 1954.

- Almorox, J., Benito, M., and Hontoria, C.: Estimation of monthly Angström–Prescott equation coefficients from measured daily data in Toledo, Spain, *Renew. Energ.*, 30, 931–936, 2005.
- Angstrom, A.: Solar and terrestrial radiation, *Q. J. Roy. Meteorol. Soc.*, 50, 121–126, doi:10.1002/qj.49705021008, 1924.
- Angstrom, A.: On computation of global radiation from records and sunshine, *Arkiv Geophysik*, 3, 471–479, 1956.
- Augustine, J. A., DeLuise, J. J., and Long, C. N.: SURFRAD-A national surface radiation budget network for atmospheric research, *B. Am. Meteorol. Soc.*, 81, 2341–2357, doi:10.1175/1520-0477(2000)081<2341:SANSRB>2.3.CO;2, 2000.
- Bider, M.: Über die Genauigkeit der Registrierungen des Sonnenscheinautographen Campbell-Stokes, *Archiv für Meteorologie, Geophysik und Bioklimatologie, Serie B*, 9, 199–230, 1958.
- Chaldecott, J. A.: Handbook of the collection relating to heat and cold, HM Stationery Office, 1954.
- Coulson, K.: Solar and Terrestrial Radiation: Methods and Measurements, Academic Press, doi:10.1016/B978-0-12-192950-3.50015-2, 1975.
- Cuevas, E., González, Y., Rodríguez, S., Guerra, J. C., Gómez-Peláez, A. J., Alonso-Pérez, S., Bustos, J., and Milford, C.: Assessment of atmospheric processes driving ozone variations in the subtropical North Atlantic free troposphere, *Atmos. Chem. Phys.*, 13, 1973–1998, doi:10.5194/acp-13-1973-2013, 2013.
- De Bruin, H. A. R., van den Hurk, B. J. J. M., and Welgraven, D.: A series of global radiation at Wageningen for 1928–1992, *Int. J. Climatol.*, 15, 1253–1272, doi:10.1002/joc.3370151106, 1995.
- Esteves, A. and de Rosa, C.: A simple method for correcting the solar radiation readings of a Robitzsch-type pyranometer, *Sol. Energy*, 42, 9–13, doi:10.1016/0038-092X(89)90125-4, 1989.
- Fröhlich, C.: History of Solar Radiometry and the World Radiometric Reference, *Metrologia*, 28, 111–115, doi:10.1088/0026-1394/28/3/001, 1991.
- García, R. D., Ramos, R., Cuevas, E., Cachorro, V. E., and de Frutos, A. M.: Status of the Izaña BSRN station, *Optica Pura y Aplicada*, 45, 51–55, 2012.
- García, R. D., Cuevas, E., García, O. E., Cachorro, V. E., Pallé, P., Bustos, J. J., Romero-Campos, P. M., and de Frutos, A. M.: Reconstruction of global solar radiation time series from 1933 to 2013 at the Izaña Atmospheric Observatory, *Atmos. Meas. Tech.*, 7, 3139–3150, doi:10.5194/amt-7-3139-2014, 2014a.
- García, R. D., Cuevas, E., García, O. E., Cachorro, V. E., Pallé, P., Bustos, J. J., Romero-Campos, P. M., and de Frutos, A. M.: Reconstruction of global solar radiation time series from 1933 to 2013 at the Izaña Atmospheric Observatory, *Atmos. Meas. Tech.*, 7, 3139–3150, doi:10.5194/amt-7-3139-2014, 2014b.
- García, R. D., García, O. E., Cuevas, E., Cachorro, V. E., Romero-Campos, P. M., Ramos, R., and de Frutos, A. M.: Solar radiation measurements compared to simulations at the BSRN Izaña station. Mineral dust radiative forcing and efficiency study, *J. Geophys. Res.-Atmos.*, 119, 179–194, doi:10.1002/2013JD020301, 2014c.
- García, R. D., García, O. E., Cuevas, E., Cachorro, V. E., Barreto, A., Guirado-Fuentes, C., Kouremeti, N., Bustos, J. J., Romero-Campos, P. M., and de Frutos, A. M.: Aerosol optical depth retrievals at the Izaña Atmospheric Observatory from 1941 to 2013 by using artificial neural networks, *Atmos. Meas. Tech.*, 9, 53–62, doi:10.5194/amt-9-53-2016, 2016.
- Garg, H. and Garg, S.: Measurement of solar radiation – I. Radiation instruments, *Renew. Energ.*, 3, 321–333, doi:10.1016/0960-1481(93)90099-3, 1993.
- Gilgen, H., Wild, M., and Ohmura, A.: Means and trends of shortwave irradiance at the surface estimated from global energy balance archive data, *J. Climate*, 11, 2042–2061, 1998.
- Gilgen, H., Roesch, A., Wild, M., and Ohmura, A.: Decadal changes in shortwave irradiance at the surface in the period from 1960 to 2000 estimated from Global Energy Balance Archive Data, *J. Geophys. Res.-Atmos.*, 114, D00D08, doi:10.1029/2008JD011383, 2009.
- Gomez-Pelaez, A. J., Ramos, R., Gomez-Trueba, V., Novelli, P. C., and Campo-Hernandez, R.: A statistical approach to quantify uncertainty in carbon monoxide measurements at the Izaña global GAW station: 2008–2011, *Atmos. Meas. Tech.*, 6, 787–799, doi:10.5194/amt-6-787-2013, 2013.
- Gorry, P. A.: General least-squares smoothing and differentiation by the convolution (Savitzky-Golay) method, *Anal. Chem.*, 62, 570–573, doi:10.1021/ac00205a007, 1990.
- Harrison, L., Michalsky, J., and Berndt, J.: Automated multifilter rotating shadow-band radiometer: an instrument for optical depth and radiation measurements, *Appl. Opt.*, 33, 5118–5125, 1994.
- Heimo, A., Vernez, A., and Wasserfallen, P.: Baseline Surface Radiation Network (BSRN), Concept and Implementation of a BSRN Station, WMO/TD, 1993.
- Hodges, G. and Michalsky, J.: Multifilter Rotating Shadowband Radiometer, Multifilter Radiometer, and Normal Incidence Multifilter Radiometer Handbook, Tech. rep., DOE/SC-ARM/TR-059, 2011.
- Holben, B., Eck, T., Slutsker, I., Tanré, D., Buis, J., Setzer, A., Vermote, E., Reagan, J., Kaufman, Y., Nakajima, T., Lavenu, F., Jankowiak, I., and Smirnov, A.: AERONET – A Federated Instrument Network and Data Archive for Aerosol Characterization, *Remote Sens. Environ.*, 66, 1–16, doi:10.1016/S0034-4257(98)00031-5, 1998.
- Kalnay, E., Kanamitsu, M., Kistler, R., Collins, W., Deaven, D., Gandin, L., Iredell, M., Saha, S., White, G., Woollen, J., Zhu, Y., Leetmaa, A., Reynolds, R., Chelliah, M., Ebisuzaki, W., Higgins, W., Janowiak, J., Mo, K. C., Ropelewski, C., Wang, J., Jenne, R., and Joseph, D.: The NCEP/NCAR 40-year reanalysis project, *B. Am. Meteorol. Soc.*, 77, 437–471, doi:10.1175/1520-0477(1996)077<0437:TNYRPS>2.0.CO;2, 1996.
- Kerr, A. and Tabony, R.: Comparison of sunshine recorded by Campbell–Stokes and automatic sensors, *Weather*, 59, 90–95, doi:10.1256/wea.99.03, 2004.
- Kipp and Zonen: Manual CSD3 Sunshine Duration Sensor, Instruction Manual, 0804 Eds., Kipp and Zonen B. V., Delft, the Netherlands, 41 pp., 2003.
- Lanzante, J. R.: Resistant, robust and non-parametric techniques for the analysis of climate data: Theory and examples, including applications to historical radiosonde station data, *Int. J. Climatol.*, 16, 1197–1226, 1996.
- Long, C. and Shi, Y.: The QCRad value added product: Surface radiation measurement quality control testing, including climatology configurable limits, Atmospheric Radiation Measurement Program Technical Report, 2006.
- Long, C. N. and Ackerman, T. P.: Identification of clear skies from broadband pyranometer measurements and calculation of down-

- welling shortwave cloud effects, *J. Geophys. Res.-Atmos.*, 105, 15609–15626, doi:10.1029/2000JD900077, 2000.
- Long, C. N. and Dutton, E. G.: BSRN Global Network recommended QC tests, V2. x, 2002.
- Maxwell, E., Wilcox, S., Cornwall, C., Marion, B., Alawaji, S., Mahfoodh, M., and Amoudi, A.: Progress Report for Annex II – Assessment of Solar Radiation Resources in Saudi Arabia 1993–1997, NREL TP, 560–25374, 1999.
- Mayer, B. and Kylling, A.: Technical note: The libRadtran software package for radiative transfer calculations – description and examples of use, *Atmos. Chem. Phys.*, 5, 1855–1877, doi:10.5194/acp-5-1855-2005, 2005.
- McArthur, L.: Baseline Surface Radiation Network (BSRN) Operations Manual V2.1, World Climate Research Programme, wmo/td-no. 1274 Edn., WCRP-121, 2005.
- Miloshevich, L. M., Vömel, H., Whiteman, D. N., and Leblanc, T.: Accuracy assessment and correction of Vaisala RS92 radiosonde water vapor measurements, *J. Geophys. Res.-Atmos.*, 114, D11305, doi:10.1029/2008JD011565, 2009.
- Moll, W.: A rapid thermopile, *K. Ned. Akad. van Wet.-B*, 16, 568–571, 1913.
- Nicolet, M.: Historical aspects of the IGY, EOS Transactions American Geophysical Union, 64, 369–369, doi:10.1029/EO064i019p00369-01, 1982.
- Ohmura, A. and Lang, H.: Secular variation of global radiation in Europe, in: *IRS*, 88, 298–301, 1989.
- Ohmura, A., Gilgen, H., Hegner, H., Müller, G., Wild, M., Dutton, E. G., Ellsworth G. and Forgan, B., Fröhlich, C., Philipona, R., Heimo, A., König-Langlo, G., McArthur, B., Pinker, R., Whitlock, C. H., and Dehne, K.: Baseline Surface Radiation Network (BSRN/WCRP): New Precision Radiometry for Climate Research, *B. Am. Meteorol. Soc.*, 79, 2115–2136, doi:10.1175/1520-0477(1998)079<2115:BSRNBW>2.0.CO;2, 1998.
- Painter, H.: The performance of a Campbell-Stokes sunshine recorder compared with a simultaneous record of the normal incidence irradiance, *Meteorol. Mag.*, 110, 102–109, 1981.
- Prescott, J.: Evaporation from a water surface in relation to solar radiation, *T. Roy. Soc. South Aust.*, 64, 114–118, 1940.
- Robitzsch: Strahlungsstudien ergebnisse, *Aero. Obs. Arbeiten*, 15 pp., 1926.
- Robitzsch: Über den bimetalaktinographen Feuss-Robitzsch, *Gerlands Beit. Geophys.*, 35, 387–394, 1932.
- Romero Campos, P. M., Marrero de la Santa Cruz, C. L., Alonso-Pérez, S., Cuevas Agulló, E., and Ortiz de Galisteo Marín, J.: Una climatología del agua precipitable en la región subtropical sobre la isla de Tenerife basada en datos de radiosondeos, vol. NTD CIAI-6, NIPO 281-12-007-5, Edita, Agencia Estatal de Meteorología, Ministerio de Medio Ambiente y Medio Marino y Rural, 2011.
- Russ, J.: *The Image Processing Handbook*, CRC Press, 1994.
- Sanchez-Lorenzo, A., Calbó, J., Wild, M., Azorin-Molina, C., and Sanchez-Romero, A.: New insights into the history of the Campbell-Stokes sunshine recorder, *Royal Meteorol. Society*, 68, 327–331, doi:10.1002/wea.2130, 2013.
- Soulayman, S. S. and Daudé, N.: A correction method for solar radiation measurements made using non-calibrated Eppley-type and Robitzsch-type pyranometers, *Appl. Energ.*, 52, 125–132, doi:10.1016/0306-2619(95)00038-T, 1995.
- Stanhill, G.: Long-term trends in, and spatial variation of, solar irradiances in Ireland, *Int. J. Climatol.*, 18, 1015–1030, 1998.
- Stanhill, G. and Cohen, S.: Global dimming: a review of the evidence for a widespread and significant reduction in global radiation with discussion of its probable causes and possible agricultural consequences, *Agr. forest Meteorol.*, 107, 255–278, doi:10.1016/S0168-1923(00)00241-0, 2001.
- Stoffel, T.: Solar infrared radiation station (SIRS) handbook, Atmospheric Radiation Measurement Program Technical Report ARM TR-025, 2005.
- Stravisi, F.: A posteriori calibration of a mechanical pyranograph, *Sol. Energy*, 36, 21–26, doi:10.1016/0038-092X(86)90056-3, 1986.
- Vignola, F., Michalsky, J., and Stoffel, T.: *Solar and infrared radiation measurements*, CRC Press, 2012.
- Wild, M.: Global dimming and brightening: A review, *J. Geophys. Res.*, 114, D00D16, doi:10.1029/2008JD011470, 2009.
- Wild, M.: Enlightening global dimming and brightening, *B. Am. Meteorol. Soc.*, 93, 27–37, doi:10.1175/BAMS-D-11-00074.1, 2012.
- Wild, M.: Decadal changes in radiative fluxes at land and ocean surfaces and their relevance for global warming, *Wiley Interdisciplinary Reviews: Climate Change*, 7, 91–107, doi:10.1002/wcc.372, 2015.
- Wild, M., Gilgen, H., Roesch, A., Ohmura, A., Long, C. N., Dutton, E. G., Forgan, B., Kallis, A., Russak, V., and Tsvetkov, A.: From dimming to brightening: Decadal changes in solar radiation at Earth's surface, *Science*, 308, 847–850, doi:10.1126/science.1103215, 2005.
- Wild, M., Ohmura, A., and Makowski, K.: Impact of global dimming and brightening on global warming, *Geophys. Res. Lett.*, 34, L04702, doi:10.1029/2006GL028031, 2007.
- Wild, M., Grieser, J., and Schär, C.: Combined surface solar brightening and increasing greenhouse effect support recent intensification of the global land-based hydrological cycle, *Geophys. Res. Lett.*, 35, L17706, doi:10.1029/2008GL034842, 2008.
- WMO: Measurement of radiation and sunshine. Guide to Meteorological Instrument and Observing Practices, 2. Edn., WMO No. 8, World Meteorological Organization, 1965.
- WMO: Guide to meteorological instruments and methods of observation, 6. Edn. WMO no. 8, Secretariat of the World Meteorological Organization, 1996.
- WMO: Commission for Instruments and Methods of Observation, Sixteenth session WMO no. 1138, Saint Petersburg, Secretariat of the World Meteorological Organization, 2014.
- Yorukoglu, M. and Celik, A. N.: A critical review on the estimation of daily global solar radiation from sunshine duration, *Energ. Convers. Manage.*, 47, 2441–2450, 2006.